Chinese Journal of Chemical Engineering 26 (2018) 1477–1484

Contents lists available at ScienceDirect

Chinese Journal of Chemical Engineering

journal homepage: www.elsevier.com/locate/CJChE

Article

Modeling investigation of geometric size effect on pervaporation dehydration through scaled-up hollow fiber NaA zeolite membranes☆

Jiacheng Wang, Peng Ye, Xuechao Gao, Yuting Zhang, Xuehong Gu *

State Key Laboratory of Materials-Oriented Chemical Engineering, College of Chemical Engineering, Nanjing Tech University, 5 Xinmofan Road, Nanjing 210009, China

ARTICLE INFO

Article history:
Received 22 October 2017
Received in revised form 24 December 2017
Accepted 18 January 2018
Available online 2 March 2018

Keywords:
Pervaporation
NaA zeolite membrane
Hollow fiber
Lumen pressure drop
Geometric parameters

ABSTRACT

A mass transfer model in consideration of multi-layer resistances through NaA zeolite membrane and lumen pressure drop in the permeate side was developed to describe pervaporation dehydration through scaled-up hollow fiber supported NaA zeolite membrane. It was found that the transfer resistance in the lumen of the permeate side is strongly related with geometric size of hollow fiber zeolite membrane, which could not be neglected. The effect of geometric size on pervaporation dehydration could be more significant under higher vacuum pressure in the permeate side. The transfer resistance in the lumen increases with the hollow fiber length but decreases with lumen diameter. The geometric structure could be optimized in terms of the ratio of lumen diameter to membrane length. A critical value of d_l/L (R_c) to achieve high permeation flux was empirically correlated with extraction pressure in the permeate side. Typically, for a hollow fiber supported NaA zeolite membrane with length of 0.40 m, the lumen diameter should be larger than 2.0 mm under the extraction pressure of 1500 Pa.

1. Introduction

Membrane pervaporation (PV) is a promising technology to separate liquid mixtures for its high separation efficiency and low energy consumption. NaA zeolite has well-defined frameworks and narrow pores (~0.42 nm) with strong hydrophilicity, which can be fabricated as PV membranes to dehydrate organic solutions with extremely high selectivity. The separation technology is particularly suited for separations of azeotropic or close-boiling aqueous-organic systems [1,2]. Since the first large-scale PV plant based on tubular NaA membranes was established by Mitsui Engineering & Shipbuilding Co. Ltd. in 1999 [3,4], considerable laboratorial and industrial efforts have been made in membrane fabrications and engineering applications [5,6].

So far, most of commercial NaA zeolite membranes are prepared on single-channel or four-channel tubular ceramic supports [7], which lead to high investment cost in membrane facilities. In order to boost industrial applications of the zeolite membrane, large packing density and high permeation flux are highly desired for zeolite membranes. Recently, hollow fiber supported zeolite membranes have been considered as an effective alternative to tubular membranes. Because of its small outer diameter and thin wall thickness, hollow fiber supported zeolite membranes exhibit ultra-high permeation flux and packing density as well. For instance, Wang *et al.* [8] prepared high performance NaA zeolite membranes on α-Al_2O_3 hollow fiber supports and achieved a permeation flux up to 9.0 $kg \cdot m^{-2} \cdot h^{-1}$ for dehydration of 90 wt% ethanol/water mixtures at 348 K. In our recent work, T-type and pure-silica MFI zeolite membranes prepared on yttria-stabilized zirconia (YSZ) hollow fibers also exhibited high permeation fluxes for organic dehydration and ethanol extraction, respectively [9,10]. To promote large-scale production, vacuum-assisted seeding method was proposed to prepare hollow-fiber NaA zeolite membranes [11]. Four-channel Al_2O_3 hollow fibers with high mechanical strength were also developed to support NaA zeolite membranes [12]. These studies suggested the technical feasibility for hollow fiber zeolite membranes applied in practical industrial processes.

Generally, the permeation flux of zeolite membranes is related with the inherent microstructure concerning zeolite membrane layer and support layer [13–18]. In our previous work, we developed a multi-layer (zeolite membrane layer/sponge-like layer/finger-like layer) series-resistance (MLSR) model to describe PV dehydrations of ethanol through hollow fiber NaA zeolite membranes [19]. It was revealed that the transfer resistance of the sponge-like region of hollow fiber support is significant since the permeation has large mean free path in the vacuum environment. On the other hand, it should be noted that the MLSR model is only suitable for analysis of lab-scale hollow fiber zeolite membranes with short length, where the pressure drop in the lumen side is negligible. For scaled-up hollow fiber NaA zeolite membranes, however, the length of hollow fiber was found to have a significant influence on the average permeation flux [11]. For example, a membrane

☆ Supported by the National Natural Science Foundation of China (21490585 and 21776128), the National High-tech R&D Program of China (2015AA03A602), the "Six Top Talents" and "333 Talent Project" of Jiangsu Province, and the Priority Academic Program Development of Jiangsu Higher Education Institutions (PAPD).
* Corresponding author.
E-mail address: xhgu@njtech.edu.cn (X. Gu).

https://doi.org/10.1016/j.cjche.2018.01.027
1004-9541/

with a length of 0.40 m only had a permeation flux of 3.87 kg·m^{-2}·h^{-1}, while a cut piece of 0.10 m showed a high flux between 5.8 and 8.1 kg·m^{-2}·h^{-1}. It was suggested that the transfer resistance through the lumen of hollow fiber was not negligible for long hollow fiber zeolite membranes. The similar influence of fiber length and lumen diameter on average permeation flux was also found in hollow fiber polyvinylidene fluoride membranes for liquid separation [20]. For pervaporation process, the effect could be more significant as a vacuum was exerted on the permeation side, in which the permeation was evacuated out of the hollow fiber lumen in low-pressure vapor. Therefore, it is of great importance to systematically explore the effect of lumen geometric size (e.g. length and diameter) on separation performance of hollow fiber zeolite membranes in consideration of industrial applications.

Herein, a mass transfer model in consideration of multi-layer resistances through NaA zeolite membrane and lumen pressure drop in the permeate side was developed to describe PV dehydration through hollow fiber supported NaA zeolite membrane. Although the viscous flow was widely used to describe the pressure-driven liquid flow in the lumen channel of hollow fiber membranes [21–24], a combination of viscous flow and Knudsen diffusion was adopted to fully account for the transport resistance of gases in the lumen. Experimental investigation was conducted to validate the modeling results. The effect of lumen geometric size on permeation flux of membrane was extensively investigated to derive the optimal lumen geometric size under specific operating conditions.

2. Theory

Fig. 1 shows a schematic diagram of the mass transfer process in a hollow fiber NaA zeolite membrane for PV dehydration. The membrane, vertically immersed in the feed solution, has a dead end at the bottom and the permeation is evacuated from the top by a vacuum pump. We previously used a MLSR model to describe component permeation through any local position on the hollow fiber membrane [19]. In the MLSR model, the cross-section of the membrane is divided into three layers, including a zeolite membrane layer, a sponge-like layer and a finger-like layer. Several assumptions are made in the model derivation as:

1. The mass flow rate through different layers should be equal at steady state;
2. The transport on the permeate and shell side follows piston flow without any radial concentration distribution and axial back-mixing;
3. The feed pressure and concentration are constant;
4. The whole process of operation is isothermal;
5. The flow in the fiber lumen is laminar and stationary.

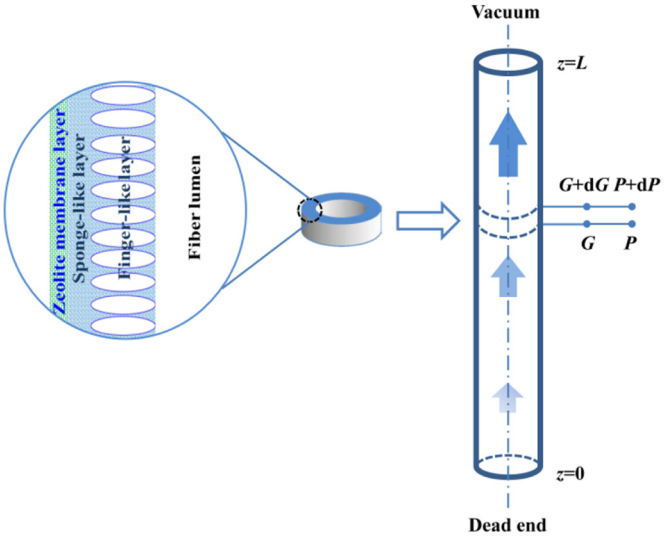

Fig. 1. A schematic diagram of pervaporation through a hollow fiber NaA zeolite membrane.

Based on the simulation of the permeate pressure gradient, it is necessary to take account of the continuous mass increase over the unit length in a differential mass balance. Subject to the above assumptions, the following equation can be written:

$$\frac{dG}{dz} = \pi d_m J \tag{1}$$

in which G is the mass flow rate of the permeate components in lumen, kg·h^{-1}; z is the length coordinate, m; d_m equals to $(d_O - d_l)/\ln(d_O/d_l)$, representing the geometric average of the fiber diameter, m; and J is the local permeation flux of components at position z, kg·m^{-2}·h^{-1}. The boundary condition for the above equation is: $z = 0$; $G = 0$.

For the compressible fluid, Thorman and Hwang [25] discovered a general pressure gradient equation based on the first order perturbation theory, where the pressure drop change caused by gas expansion can be ignored when the wall Reynolds number is far less than 1, just as the membrane separation process, so that the pressure drop can be expressed by the differential form of the Hagen–Poiseuille equation for laminar flow. Given the low pressure limits of the permeate vapor in the permeate channel, ideal gas equation of state ($P^P V = G_{Vis}RT/M$) is applied, where the volume flow rate (V), equals to $\pi d_l^2 \bar{v}/4$, m^3·h^{-1}, and M is the molecular weight of the permeate vapor, kg·mol^{-1}. Thus, the mass flow rate for the viscous can be derived as:

$$G_{Vis} = -\frac{\pi d_l^4 M P^P}{128RT\mu}\frac{dP^P}{dz} \tag{2}$$

On account of the low pressure condition in the permeate side, it is necessary to calculate the Knudsen number to define the flow regime for the permeate vapor flowing through the lumen by

$$Kn = \frac{k_B T}{\sqrt{2}\pi d_p^2 PL} \tag{3}$$

where k_B is the Boltzmann constant; T corresponds to the thermodynamic temperature, K; d_p represents the particle hard-shell diameter, m; P is the total pressure, Pa; and L equals to the representative physical length scale, m. The obtained Knudsen number is about 0.02, which is between 0.01 and 0.5, so the flow regime belongs to the transitional region and the Knudsen diffusion should be included in the model [26–31]. The flow rate contribution from the Knudsen diffusion is described as:

$$G_{Kn} = -\frac{\pi d_l^3 M}{12RT}\sqrt{\frac{8RT}{\pi M}}\frac{dP^P}{dz} \tag{4}$$

Therefore, the total flow rate can be seen as a superposition of the two fluxes.

$$G = G_{Vis} + G_{Kn} \tag{5}$$

The pressure drop for the permeate side of hollow fiber as follows:

$$\frac{dP^P}{dz} = -\left(\frac{\pi d_l^4 M P^P}{128RT\mu} + \frac{\pi d_l^3 M}{12RT}\sqrt{\frac{8RT}{\pi M}}\right)^{-1} G \tag{6}$$

where μ can be regarded as a constant parameter for the gas viscosity is hardly affected by the pressure. The boundary condition is: $z = L$; $P^P = P_L$.

The local permeation flux at position z in the membrane system is modeled by a MLSR mass transfer model. For the zeolite membrane

layer, the permeation flux of each component is described by a generalized Maxwell–Stefan equation by:

$$J_{Z,w} = \frac{\rho_Z M_w D_w(0) q_M}{\delta_Z}\left(\frac{K_w P_w^F}{1+K_w P_w^F} - \frac{K_w P_w^{int,1}}{1+K_w P_w^{int,1}}\right) \tag{7}$$

$$J_{Z,e} = \frac{\rho_Z M_e D_e(0) q_M}{\delta_Z}\left(\frac{1+K_e P_e^F}{1+K_w P_w^F}\right)\left(\frac{K_e P_e^F}{1+K_w P_w^F} - \frac{K_e P_e^{int,1}}{1+K_w P_w^{int,1}}\right) + \frac{M_e D_e(0)}{M_w D_w(0)}\frac{K_e P_e^F}{1+K_w P_w^F} J_{Z,w} \tag{8}$$

Eqs. (7) and (8) represents steady-state permeation flux of component water and ethanol ($J_{Z,w}$ and $J_{Z,e}$) through the zeolite membrane, respectively. The adsorption and diffusion parameters were obtained by molecular simulation, and the detailed simulation methods were described in our previous work [19,32].

The permeation flux of the mixture through the hollow fiber support is characterized by the slip flow, in which the mass flux of component *i* through the sponge-like region and the finger-like region is described by Eqs. (9) and (10) for Knudsen diffusion and viscous flow, respectively.

$$J_{S,i} = \frac{\varepsilon M_i}{\tau RT\delta_S}\left[\frac{d_p}{3}\sqrt{\frac{8RT}{\pi M_i}}\left(P_i^{int,1} - P_i^{int,2}\right) + \frac{\overline{P}_i {d_p}^2}{32\eta}\left(P_{Total}^{int,1} - P_{Total}^{int,2}\right)\right] \tag{9}$$

$$J_{F,i} = \frac{\varepsilon M_i}{\tau RT\delta_F}\left[\frac{d_p}{3}\sqrt{\frac{8RT}{\pi M_i}}\left(P_i^{int,2} - P_i^{P}\right) + \frac{\overline{P}_i {d_p}^2}{32\eta}\left(P_{Total}^{int,2} - P_{Total}^{P}\right)\right] \tag{10}$$

Since the permeate pressure profile across the hollow fiber is unknown, Eqs. (1) and (6) contain a two-point boundary value problem. To solve the differential equations, a trial-and-error shooting method is adopted to convert the boundary value problem into an initial value problem. In other words, a value of P^P at $z = 0$ is assumed and integrated to $z = L$. The obtained value of P^P at $z = L$ is subsequently compared with the appointed boundary condition, and then the integration is repeated with a new guess of P^P at $z = 0$ until the convergence is achieved. Afterwards, the permeate pressure profile and the mass flow rate inside the lumen of hollow fiber membrane are eventually determined. By combining the MLSR permeation equations with the mass transfer model inside the lumen, a general equation system is readily obtained to estimate the pressure drop in the lumen of hollow fiber NaA zeolite membrane and the water permeation flux at different positions. The average permeation flux (J_{av}) through the whole hollow fiber membrane can be obtained by integrating the local permeation flux in *z*-axial direction.

$$J_{av} = \frac{1}{L}\int_0^L J dz \tag{11}$$

The above equations are derived based on the laminar flow in the lumen of hollow fiber NaA zeolite membrane, which should be rationalized by evaluating the Reynolds number. Obviously, the maximum *z*-axis Reynolds number is located at the extraction point for the corresponding flow velocity is the largest, which can be calculated by Eq. (12). It is evident that the assumption of the laminar flow in the lumen is applicable if the maximum Reynolds number in *z*-axis is less than 2300.

$$Re_{max} = \frac{\rho v_{max} d_l}{\mu} = \frac{4G_{max}}{\pi\mu d_l} \tag{12}$$

3. Experimental

The NaA zeolite membranes used in this study were hydrothermally synthesized on the outer surfaces of the α-Al_2O_3 hollow fiber supports as the separation layer. The detailed preparation of the hollow fiber NaA zeolite membranes was described in our previous work [11]. The mean pore size of the support was measured by a gas bubble pressure instrument, and the porosity and tortuosity were characterized by a mercury porosimeter (PoreMaster GT60, Quantachrome Instruments). The separation performances of NaA zeolite membranes were evaluated by PV dehydration of 95 wt% ethanol/water at 348 K. In the PV experiments, ethanol/water feed mixture externally flowed over the surface of hollow fiber membrane under atmospheric pressure, and the lumen of the hollow fiber was extracted by a vacuum pump through a vacuum line, where the pressure was maintained around 200 Pa throughout the experiment. The permeated vapor mixture was collected by cold traps cooled by liquid nitrogen. The feed and permeate composition were analyzed by a gas chromatograph (GC-2014A, Shimadzu) with a thermal conductivity detector (TCD) and a packed column of Parapak-Q (Alltech). The PV performance is determined by permeation flux (J_{exp}) and separation factor ($\alpha_{w/e}$), defined as:

$$J_{exp} = \frac{m_i}{A\Delta t} \tag{13}$$

$$\alpha_{w/e} = \frac{Y_w/X_w}{Y_e/X_e} \tag{14}$$

where m_i is the mass of permeate *i*, kg; *A* represents the effective membrane area, m^2; Δt is the permeation time, h; X_w and X_e are mass fractions of water and ethanol in the feed; Y_w and Y_e correspond to mass fractions in the permeate.

4. Results and Discussion

4.1. Model validation

We have previously observed length-dependence of average water flux for hollow fiber supported NaA zeolite membrane, which was attributed to driving force loss along the permeate lumen side [11]. To validate the mathematic model, we further investigated the effect of membrane length on water permeation flux by both experimental and modeling. A hollow fiber NaA zeolite membrane with 20 cm length was cut gradually and evaluated by PV experiment. The thickness of the membrane layer was 8 μm. The porosity and tortuosity of the support were 45.2% and 2, respectively; the mean pore sizes for the sponge-like and finger-like layer were 0.54 μm and 2.75 μm, respectively, and the corresponding thicknesses were 0.16 mm and 0.26 mm, respectively. Fig. 2 presents the calculated and experimental water fluxes through the membranes used for dehydration of 95 wt.% ethanol/water at 348 K. As can be seen, the predicted permeation fluxes are slightly higher than the experimental results. However, the dependences of permeation flux over membrane length are quite similar. For instance, when the membrane length increases from 0.05 to 0.20 m, the experimental water flux decreases from 6.35 $kg\cdot m^{-2}\cdot h^{-1}$ to 4.27 $kg\cdot m^{-2}\cdot h^{-1}$, which is similar to the decrement in the model prediction, i.e., from 7.14 $kg\cdot m^{-2}\cdot h^{-1}$ to 5.90 $kg\cdot m^{-2}\cdot h^{-1}$ by using a slip flow in the lumen. The decreasing tendency can be explained by the driving force loss along the permeate side. As the membrane length is extended, more products accumulate in the lumen, which requires a larger pressure drop to extract the products, i.e., the lumen bottom pressure becomes higher, thereby decreasing the pressure drop across the membrane layer. The above results indicate the intrinsic behavior of the fluid transport in the supported membrane is essentially captured in the developed model.

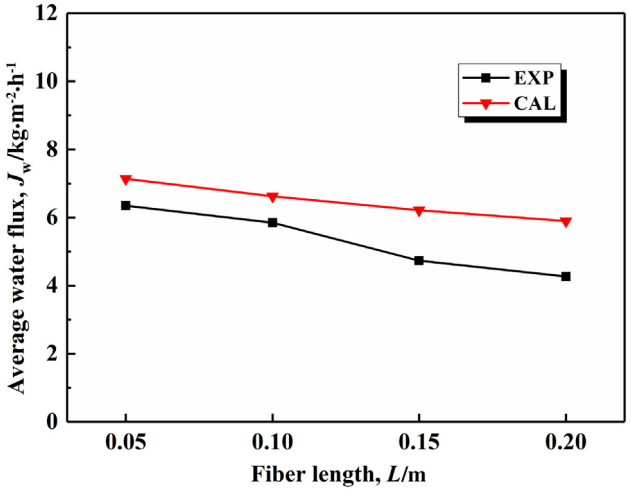

Fig. 2. Comparison of calculated and experimental water fluxes under different lengths of hollow fiber NaA zeolite membrane for separation of 95 wt% ethanol/water mixture at 348 K.

The Reynolds numbers calculated by Eq. (12) are summarized in Table 1. Since all of the values are below 2300, the initial assumption of laminar flow in the lumen is physically solid. Therefore, it can be concluded that despite in the transitional region, the viscous flow can be treated as the dominated term for describing the mass transfer in the lumen of the hollow fibers.

Table 1
Re_{max} for different fiber lengths and lumen diameters (T = 348 K, P_L = 200 Pa)

L/m	d_l/mm				
	0.5	1.0	1.5	2.0	2.5
0.05	48.30	47.77	45.44	43.60	42.52
0.10	73.75	87.18	86.71	85.21	83.84
0.15	86.62	119.45	124.01	123.41	123.22
0.20	92.93	145.74	157.67	159.68	160.87
0.25	95.98	167.07	188.00	193.68	196.88
0.30	97.43	184.29	215.30	225.55	231.30
0.35	98.11	196.73	238.46	255.39	263.04
0.40	98.44	209.25	261.84	283.33	295.59
0.45	98.59	216.68	280.04	309.46	324.21
0.50	98.66	225.21	299.24	333.90	354.22

4.2. Influence of fiber length

Fig. 3 depicts the pressure and local permeance profiles of water along the lumen as a function of fiber length. The general microstructure parameters of the hollow fiber NaA zeolite membrane used for calculation are listed in Table 2, which are also applied in the discussion sections that follow. The hollow fiber has an inner diameter of 1 mm. As can be seen, the permeate pressure and local permeation flux of water vary with z-axial positions of hollow fibers. Pressure is built up in permeate sides to provide driving forces for product extraction. The lowest permeate pressure, leading to the highest local water flux, occurs in the extraction position. Interestingly, although the lumen exit pressure ($z = L$) is constant, the dead end pressure ($z = 0$) increases with the extension of the fiber length (Fig. 3a). For instance, when the fiber length increases from 0.05 to 0.5 m, the pressure at the dead end climbs from 1273 to 7734 Pa, which causes the local water permeation flux at the dead end decreasing from 6.90 to 2.16 kg·m^{-2}·h^{-1}, as shown in Fig. 3b. The larger lumen pressure drop of water between the dead end and exit suggests more permeate accumulated in the lumen, and a stronger transport resistance is thus observed [33].

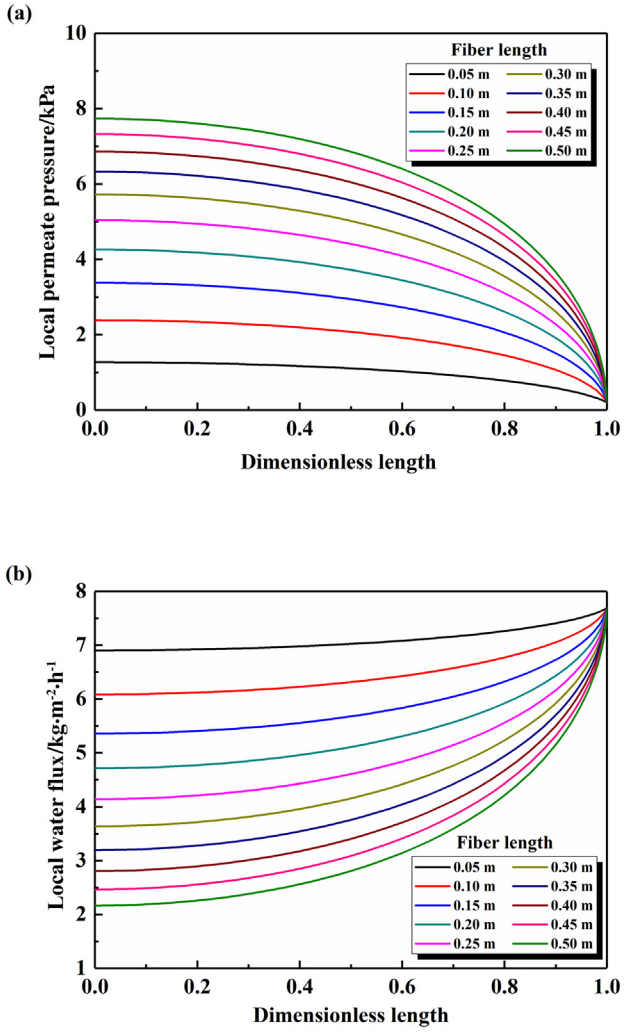

Fig. 3. (a) Modeled permeate pressure distribution in the lumen and (b) local permeation flux profile of water along the axial position of hollow fiber zeolite membrane with different lengths for separation of 95 wt% ethanol/water mixture (T = 348 K, d_l = 1 mm, P_L = 200 Pa).

The average permeation flux as a function of membrane length is illustrated in Fig. 4. As shown in the figure, the average water permeation flux is almost halved (from 7.12 kg·m^{-2}·h^{-1} to 3.35 kg·m^{-2}·h^{-1}) when the hollow fiber membrane extends from 0.05 m to 0.5 m. The results suggest that the impact of membrane length is more significant for the scaled up products. It can be seen that the ethanol permeation flux maintains nearly constant at around 0.5 kg·m^{-2}·h^{-1}, probably due to its low permeability, which allows a relatively smaller partial pressure drop in the lumen. As discussed above, the highest local water permeation flux is located at the lumen exit of hollow fiber-supported NaA zeolite membrane. Fig. 4 also presents the ratio of average permeation flux to the local permeation flux at the lumen exit. It can be seen that the

Table 2
Microstructure parameters of the hollow fiber NaA zeolite membrane for modeling

Microstructure parameters	Value
Zeolite layer thickness/μm	7.5
Hollow fiber support porosity/%	50
Hollow fiber support tortuosity	2
Sponge-like layer mean pore size/μm	0.27
Sponge-like layer thickness/mm	0.12
Finger-like layer mean pore size/μm	5
Finger-like layer thickness/mm	0.3

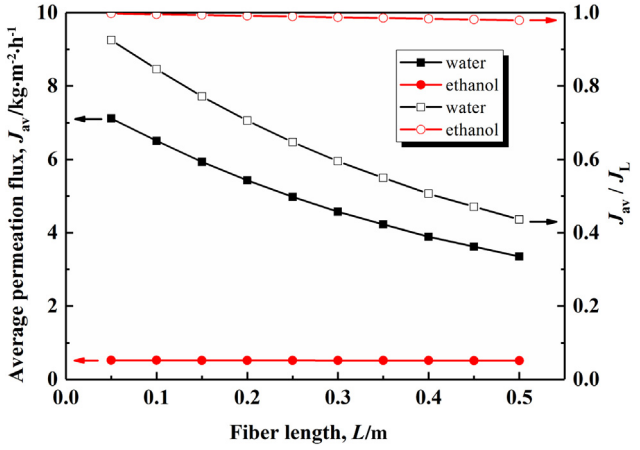

Fig. 4. Modeled average permeation flux and the ratio of average permeation flux to local permeation flux at lumen exit of hollow fiber NaA zeolite membrane with different membrane lengths for separation of 95 wt% ethanol/water mixture (T = 348 K, d_I = 1 mm, P_L = 200 Pa).

ratio varies from 0.93 to 0.44 for water permeation flux when the fiber length increases from 0.05 m to 0.5 m. For the hollow fiber NaA zeolite membrane with a length of 0.5 m, over 60% of membrane area has the local water flux lower than the average water flux. This means that the long hollow fiber zeolite membrane cannot display high separation performance in the region nearby the dead end, suggesting the necessity to optimize the geometric size of scaled-up hollow fiber membranes to obtain high permeation performance.

4.3. Influence of lumen diameter

According to Eq. (6), the lumen diameter is another geometric parameter to affect the mass transfer resistance in the permeate side of hollow fiber zeolite membrane. Fig. 5 shows the pressure distribution in the permeate side and the local permeation flux profile of water along axial direction for hollow fiber NaA zeolite membranes with different lumen diameter. The separation are operated for dehydration of 95 wt.% ethanol/water mixture at 348 K and the hollow fiber membranes have a fixed length of 0.10 m. All the other microstructural parameters of hollow fiber NaA zeolite membrane are summarized in Table 2. As expected, the lumen pressure for all the membranes gradually reduces along the axial direction from the dead end to the exit. However, the pressure gradient becomes steeper for smaller lumen dimensions, implying higher transport resistance built up in the lumen side. For instance, when the lumen diameter reduces from 2 mm to 1 mm, the pressure at the dead end increases from 868 Pa to 2387 Pa. Accordingly, the local water flux drop between the dead end and exit varies from 0.49 kg·m^{-2}·h^{-1} to 1.60 kg·m^{-2}·h^{-1}, which suggests that more uniform permeation flux exists along axial coordinate for the enlarged lumen. Therefore, the enlargement of the lumen diameter is helpful to maintain a high separation performance of the hollow fiber zeolite membrane.

Fig. 6 illustrates variation of average permeation fluxes with different lumen diameters, and the ratio of average permeation flux to local permeation flux at lumen exit. As suggested, when the lumen diameter increases from 0.5 mm to 1.0 mm, the average water flux readily increases from 4.46 kg·m^{-2}·h^{-1} to 6.51 kg·m^{-2}·h^{-1}. However, only a slight increase of the average water flux (from 7.09 kg·m^{-2}·h^{-1} to 7.47 kg·m^{-2}·h^{-1}) is achieved for the lumen diameter from 1.5 mm to 2.5 mm. The average water fluxes are very close to the water flux at the exit. Accordingly, it can also be seen in Fig. 6 that the ratio of average permeation flux to local permeation flux at lumen exit varies from 0.58 to 0.85 for water when the lumen diameter increases from 0.5 mm to 1.0 mm. For a further diameter enlargement from 1.5 mm to 2.5 mm, the permeation ratio varies from 0.92 to 0.97. The result suggests that

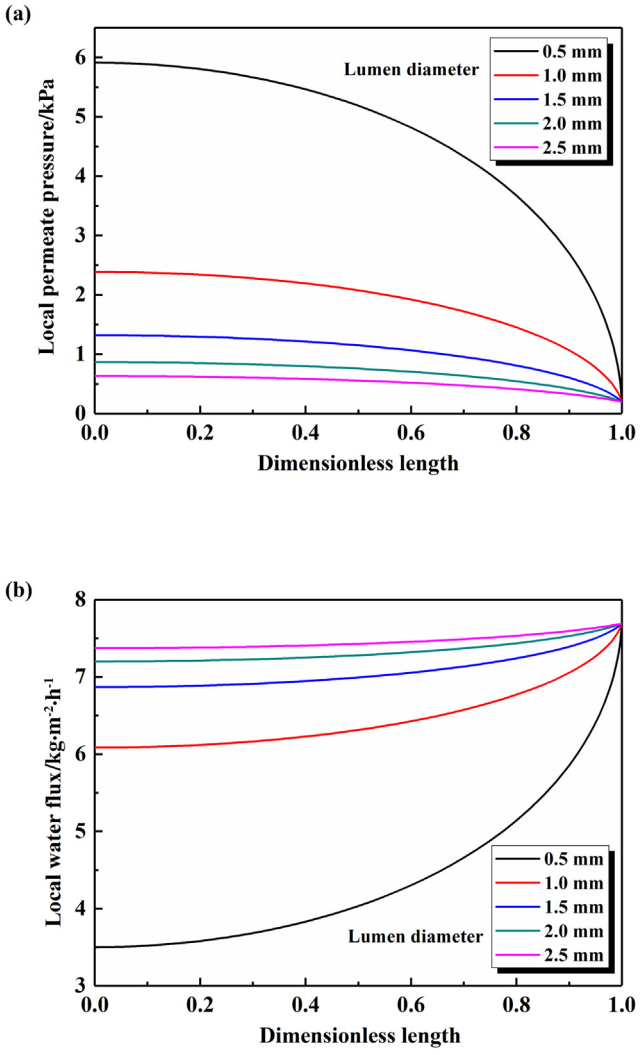

Fig. 5. Modeled pressure distribution in the permeate side (a) and water permeation flux profile (b) along the axial coordinates of hollow fiber NaA zeolite membrane with different lumen diameters for separation of 95 wt% ethanol/water mixture (T = 348 K, L = 0.10 m, P_L = 200 Pa).

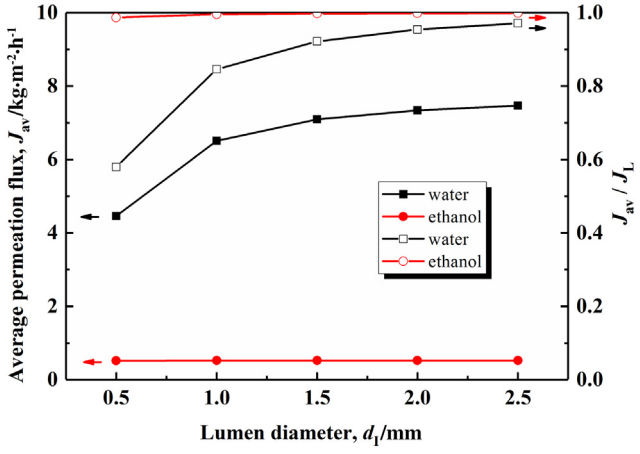

Fig. 6. Modeled results for the effect of lumen diameter on the average permeation flux and the ratio of average permeation flux to local permeation flux at lumen exit of hollow fiber NaA zeolite membrane for separation of 95 wt% ethanol/water mixture (T = 348 K, L = 0.10 m, P_L = 200 Pa).

the mass transfer resistance in the lumen is negligible for lumen diameter larger than 1.5 mm. An increase of lumen diameter attenuates the pressure accumulates inside the fiber lumen. However, the lumen diameters should not be too big in consideration of the membrane packing density.

4.4. Influence of extraction pressure

Fig. 7 depicts the influence of extraction pressure (P_L) on the mean transmembrane pressure and average permeation flux for separation of 95 wt% ethanol/water mixture at 348 K. The mean transmembrane pressure is indicated by the logarithmic mean value of transmembrane pressure (P_m) at the dead end and exit of the hollow fiber NaA zeolite membrane which is calculated as:

$$P_m = \frac{\left(P_i^F - P_{i,L}\right) - \left(P_i^F - P_{i,0}\right)}{\ln\left[\left(P_i^F - P_{i,L}\right)/\left(P_i^F - P_{i,0}\right)\right]} \quad (15)$$

where P_i^F, $P_{i,0}$ and $P_{i,L}$ are the partial pressures of component i at feed side, at the dead end of permeate side and at the exit of permeate side, respectively. For the further investigation of the effect of the extraction pressures on the flux, simulations under the pressure condition from 200 Pa to 10000 Pa were conducted. When the extraction pressure increases, the mean transmembrane pressure of water slowly decreases at first before starting a steep drop afterwards. Such an effect becomes more significant for the average permeation flux at P_L below 1500 Pa. In Fig. 7b, besides the linearly decreasing of average water flux for P_L above 1500 Pa, a minor decrement from 6.5 $kg \cdot m^{-2} \cdot h^{-1}$ to 6.1 $kg \cdot m^{-2} \cdot h^{-1}$ occurs for P_L increasing from 200 Pa to 1500 Pa, leading to an almost flat curve. This result suggests that the applied extraction pressure has a great influence on water transfer in the fiber lumen. At low extraction pressures, for example $P_L = 200$ Pa, the permeate pressure at the dead end is about 10 times higher than the exerted extraction pressure. Further, any further reduction of P_L to less than 200 Pa hardly improves the average permeation flux due to the weak dependence of water permeation flux at low extraction pressures [21]. For ethanol permeation, the effect of extraction pressure on the average permeation flux is almost negligible due to its low permeability. It should be noted that the pressure dependence of permeation flux is also related with the geometric dimension of hollow fiber, which is discussed below. The trends observed are expected to have guiding significance for scaled-up application of hollow fiber NaA zeolite membranes.

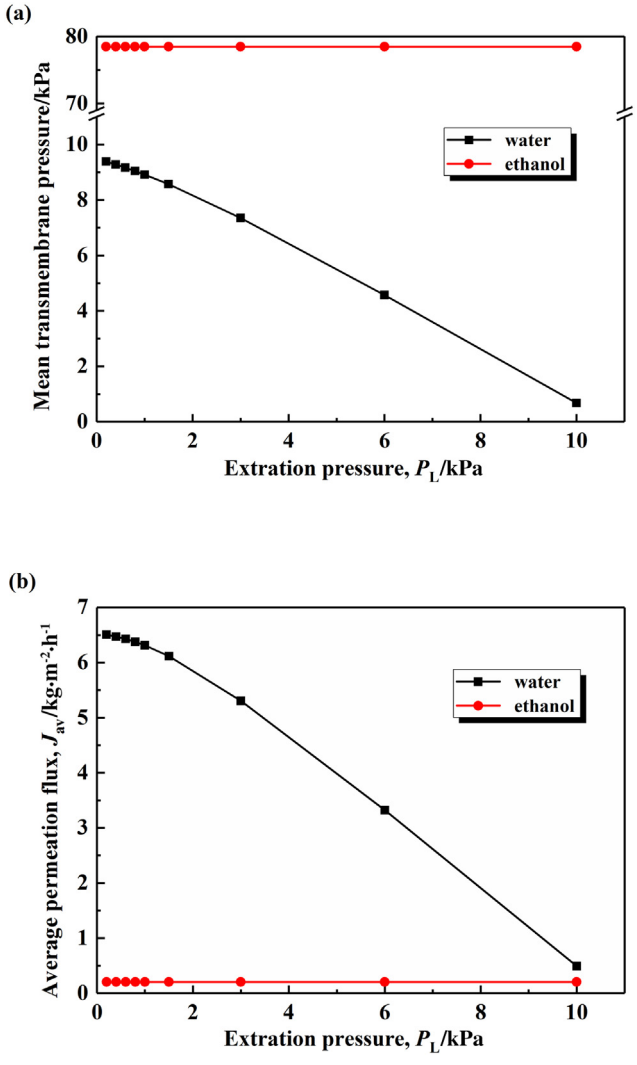

Fig. 7. (a) Variation of mean transmembrane pressure and (b) average permeation flux for separation of 95 wt% ethanol/water mixture versus different extraction pressures ($T = 348$ K, $d_l = 1$ mm, $L = 0.10$ m).

4.5. Synergistic effect

Since the fiber length, lumen diameter and extraction pressure are influential on the water permeation, we further consider the synergistic effect by the three factors. Using the model microstructure parameters provided in Table 2, Fig. 8 describes the average water permeation flux as functions of lumen diameter and fiber length for separation of 95 wt% ethanol/water mixture at 348 K. It can be seen that the average water permeation flux varies with both lumen diameter and fiber length. It is suggested that for scaled-up hollow fiber membranes with extended length, and the lumen size should be enlarged to maintain high permeation performance. It seems that the permeation flux is more sensitive to lumen diameter than fiber length. For a fiber with a length of 0.4 m and a lumen diameter of 1.0 mm, the achieved average water flux is about 3.90 $kg \cdot m^{-2} \cdot h^{-1}$. When the lumen diameter is doubled to 2.0 mm, the average water flux increases to 6.14 $kg \cdot m^{-2} \cdot h^{-1}$. On the other hand, the fiber length should be reduced to about 0.125 m to have a similar flux. This is primarily due to the inversely proportion of pressure gradient to the fourth power of lumen radius based on the Hagen–Poiseuille law. Owing to the higher pressure gradient in the narrow lumen, the nonuniform degree of permeate flux is also enhanced.

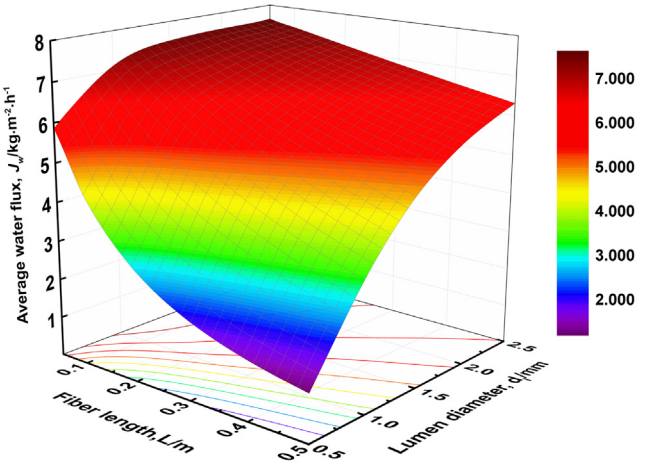

Fig. 8. Modeled result for the effect of fiber length and lumen diameter on the average water flux for separation of 95 wt% ethanol/water mixture ($T = 348$ K, $P_L = 200$ Pa).

Fig. 9 shows the average water permeation flux versus the ratio of lumen diameter to fiber length (d_l/L) for different extraction pressures. As suggested, the average permeation flux increases with d_l/L for each case, and the average permeation flux could continuously reach up to the maximum value equaling to the local permeation flux at the exit. Further, the average permeation flux demonstrates a significant variation at low d_l/L before the flattening curves at high d_l/L. For instance, at a low extraction pressure of 200 Pa, the average water flux increases from 1.31 $kg\cdot m^{-2}\cdot h^{-1}$ to 6.16 $kg\cdot m^{-2}\cdot h^{-1}$ when d_l/L becomes from 0.001 to 0.01. On the contrary, the flux changed slightly between 7.12 and 7.61 $kg\cdot m^{-2}\cdot h^{-1}$ for d_l/L varying from 0.013 to 0.05. It is suggested that the effect of transfer resistance in the permeate side is not significant when d_l/L exceeds a critical value (R_c). From the viewpoint of practical application, the critical d_l/L is important to achieve both high separation performance and low fabrication cost for a membrane module. In this work, we select different R_c values for each extraction pressure, where the corresponding fluxes are about 80% of the local permeation flux at the exit. The critical d_l/L can be used for designing geometric size of hollow fiber. For the hollow fiber with d_l/L larger than R_c, although a high permeation performance is achieved, the membrane packing density is sacrificed.

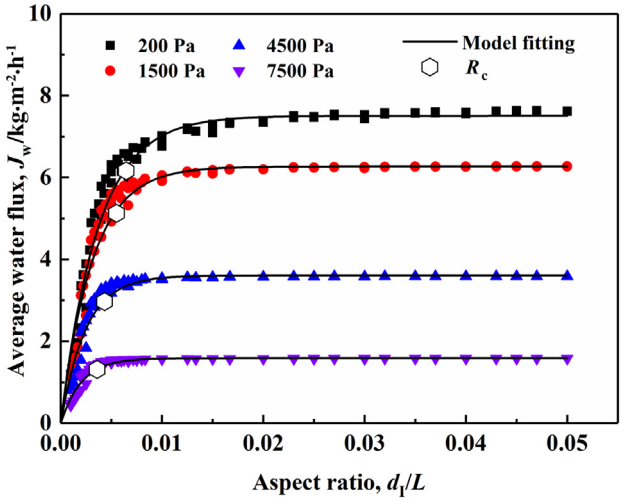

Fig. 9. Variation and empirical nonlinear fitting of the aspect ratio effect of lumen diameter to hollow fiber length on the average water flux at different extraction pressures for separation of 95 wt% ethanol/water mixture at $T = 348$ K, where the hexagon symbols (⬡) represent the critical ratio of d_l/L (R_c) derived from empirical nonlinear fittings.

To quantitatively analyze the relationship between R_c and extraction pressure, nonlinear fitting is performed for the given data. For a certain extraction pressure, the average water flux of J_w varying with d_l/L matches the formula below:

$$J_w = J_m\left(1-e^{-k\frac{d_l}{L}}\right) \tag{16}$$

where J_m and k correspond to the maximum flux and coefficient, respectively. The obtained diagrams for the fitting functions are also plotted in Fig. 9, and the fitted model parameters are summarized in Table 3. Good agreements are obtained for each extraction pressure with a high coefficient of determination (r^2) of 0.9.

Table 3
The obtained parameters for Eq. (17) by mathematic fitting

P_L/Pa	J_m/kg·m^{-2}·h^{-1}	k	$R_c \times 10^3$
200	6.16	273.99	5.87
1500	5.13	321.01	5.01
4500	2.97	409.69	3.93
7500	1.31	492.92	3.27

Since the current empirical model accurately describes the relationship of flux and d_l/L under all the conditions of extraction pressures, the theoretical values of R_c for each extraction pressure can be estimated from Eq. (17) based on the aforementioned assumption that 80% of the theoretical maximum flux should be required in practical application. The values of R_c are also marked in Fig. 9. As expected, the value of R_c decreases with increases in P_L. For instance, R_c reduces from 0.00587 to 0.00327 when P_L increases from 200 Pa to 7500 Pa. A fitting is also performed to describe the relationship between the parameters R_c and P_L. Considering R_c is exceptionally determined by k in a form of $R_c = 1.61/k$, only the relationship between k and P_L is explored. For the purpose of simplicity, liner fitting models are conducted for the estimation of k, which provides a new approach to predict R_c. The eventual expression for R_c ($r^2 > 0.99$) is shown as follows:

$$R_c = \frac{1.61}{272.057 + 2.97\times10^{-2}P_L} \tag{17}$$

For an extraction pressure of 1500 Pa in practical application, the optimal lumen diameter would be no less than 2.0 mm when the fiber length rises to 0.4 m in order to achieve enough permeation flux for dehydration of ethanol.

5. Summary and Conclusions

A mass transfer mathematical model based on the combination of lumen pressure drop equation using slip flow and a multi-layer (zeolite membrane layer/sponge-like layer/finger-like layer) series-resistance model is developed to investigate PV dehydration through scaled-up hollow fiber NaA zeolite membranes. A parametric analysis shows that the dimensions of the hollow fiber (lumen diameter and fiber length) and extraction pressure have significantly synergistic effect on the overall pervaporation performance of a hollow fiber zeolite membrane. Therefore, the geometric parameters of hollow fiber should be optimized in order to achieve high permeation flux. The model results indicate that an increase in lumen diameter could improve the permeation flux of hollow fiber NaA zeolite membranes. In contrast, an increase in the extraction pressure and fiber length could cause the decrement of the average permeation flux. To facilitate the application of the simulation discoveries in practical industries, the critical value of d_l/L, R_c, which yields 80% of the theoretical maximum flux, is correlated with P_L, and an inverse relationship is derived. The results suggest a reasonable lumen diameter for a certain fiber length is beneficial to maintain high pervaporation performance. In general, the developed model can be extended to the other types of feed solutions and membranes by adjusting the corresponding adsorption and diffusion parameters.

Nomenclature

A_I	cross sectional area of lumen, m^2
D_s	self-diffusivity, $m^2\cdot s^{-1}$
d_I	inside diameter of hollow fiber NaA zeolite membrane, m
d_O	outside diameter of hollow fiber NaA zeolite membrane, m
d_p	pore diameter, m
G	mass flow rate, $kg\cdot h^{-1}$
J	permeation flux, $kg\cdot m^{-2}\cdot h^{-1}$
J_m	maximum average water flux, $kg\cdot m^{-2}\cdot h^{-1}$
K	adsorption constant, Pa^{-1}
k	empirical constant (dimensionless)
L	hollow fiber length, m
M	molecular weight, $kg\cdot mol^{-1}$
P	pressure, Pa
P_L	pressure at the exit of hollow fiber NaA zeolite membrane, Pa
q_M	saturated loading, $mol\cdot kg^{-1}$
R	gas constant (8.314 $Pa\cdot m^{-3}\cdot mol^{-1}\cdot K^{-1}$)
R_c	critical value of d_l/L (dimensionless)
V	volume flow rate, $m^3\cdot h^{-1}$

z	length coordinate at any point, m
$\alpha_{w/e}$	water/ethanol separation factor
γ	activity coefficient
δ	thickness, m
ε	support porosity
η	viscosity, Pa·s
ρ_Z	density of zeolite layer, kg·m^{-3}
τ	support tortuosity
v	axial flow rate, m·h^{-1}

Subscripts

av	average value
e	ethanol
F	finger-like layer
I	inner side
Kn	Knudsen flow
max	maximum
O	outer side
S	sponge-like layer
Vis	Viscous flow
w	water
Z	NaA zeolite layer

Superscripts

F	feed side
int,1	zeolite/support interface
int,2	sponge-like/finger-like interface
P	permeate side

References

[1] P.D. Chapman, T. Oliveira, A.G. Livingston, K. Li, Membranes for the dehydration of solvents by pervaporation, *J. Membr. Sci.* 318 (2008) 5–37.

[2] X. Feng, R.Y.-M. Huang, Liquid separation by membrane pervaporation: A review, *Ind. Eng. Chem. Res.* 36 (1997) 1048–1066.

[3] U. Caro, M. Noack, A. Peter, Zeolite membranes: From the laboratory scale to technical applications, *Adsorption* 11 (2005) 215–227.

[4] Y. Morigami, M. Kondo, J. Abe, H. Kita, K. Okamoto, The first large-scale pervaporation plant using tubular-type module with zeolite NaA membrane, *Sep. Purif. Technol.* 25 (2001) 251–260.

[5] J. Gascon, F. Kapteijn, B. Zornoza, V. Sebastián, C. Casado, J. Coronas, Practical approach to zeolitic membranes and coatings: State of the art, opportunities, barriers, and future perspectives, *Chem. Mater.* 24 (2012) 2829–2844.

[6] N. Rangnekar, N. Mittal, B. Elyassi, J. Caro, M. Tsapatsis, Zeolite membranes — A review and comparison with MOFs, *Chem. Soc. Rev.* 44 (2015) 7128–7154.

[7] S. Sommer, B. Klinkhammer, M. Schleger, T. Melin, Performance efficiency of tubular inorganic membrane modules for pervaporation, *AIChE J.* 51 (2005) 162–177.

[8] Z. Wang, Q. Ge, J. Shao, Y. Yan, High performance zeolite LTA pervaporation membranes on ceramic hollow fibers by dipcoating–wiping seed deposition, *J. Am. Chem. Soc.* 131 (2009) 6910–6911.

[9] X. Shu, X. Wang, Q. Kong, X. Gu, N. Xu, High-flux MFI zeolite membrane supported on YSZ hollow fiber for separation of ethanol/water, *Ind. Eng. Chem. Res.* 51 (2012) 12073–12080.

[10] X. Wang, Y. Chen, C. Zhang, X. Gu, N. Xu, Preparation and characterization of high-flux T-type zeolite membranes supported on YSZ hollow fibers, *J. Membr. Sci.* 455 (2014) 294–304.

[11] Y. Liu, X. Wang, Y. Zhang, Y. He, X. Gu, Scale-up of NaA zeolite membranes on α-Al_2O_3 hollow fibers by a secondary growth method with vacuum seeding, *Chin. J. Chem. Eng.* 23 (2015) 1114–1122.

[12] D. Liu, Y. Zhang, J. Jiang, X. Wang, C. Zhang, X. Gu, High-performance NaA zeolite membranes supported on four-channel ceramic hollow fibers for ethanol dehydration, *RSC Adv.* 5 (2015) 95866–95871.

[13] F. Peng, F. Pan, D. Li, Z. Jiang, Pervaporation properties of PDMS membranes for removal of benzene from aqueous solution: Experimental and modeling, *Chem. Eng. J.* 114 (2005) 123–129.

[14] S. Chaturabul, W. Srirachat, T. Wannachod, P. Ramakul, U. Pancharoen, S. Kheawhom, Separation of mercury(II) from petroleum produced water via hollow fiber supported liquid membrane and mass transfer modeling, *Chem. Eng. J.* 265 (2015) 34–46.

[15] M. Pera-Titus, C. Fité, V. Sebastián, E. Lorente, J. Llorens, F. Cunill, Modeling pervaporation of ethanol/water mixtures within "real" zeolite NaA membranes, *Ind. Eng. Chem. Res.* 47 (2008) 3213–3224.

[16] N. Mittal, P. Bai, A. Kelloway, J.I. Siepmann, P. Daoutidis, M. Tsapatsis, A mathematical model for zeolite membrane module performance and its use for techno-economic evaluation of improved energy efficiency hybrid membrane-distillation processes for butane isomer separations, *J. Membr. Sci.* 520 (2016) 434–449.

[17] M. Weyd, H. Richter, P. Puhlfürß, I. Voigt, C. Hamel, A. Seidel-Morgenstern, Transport of binary water-ethanol mixtures through a multilayer hydrophobic zeolite membrane, *J. Membr. Sci.* 307 (2008) 239–248.

[18] X. Gao, G. Ji, L. Peng, X. Gu, L. Chen, Pore-neck resistance to light gases in a microporous BTESE-derived silica: A comparison of membrane and xerogel powder, *J. Membr. Sci.* 531 (2017) 36–46.

[19] P. Ye, Y. Zhang, H. Wu, X. Gu, Mass transfer simulation on pervaporation dehydration of ethanol through hollow fiber NaA zeolite membranes, *AIChE J.* 62 (2016) 2468–2478.

[20] X. Li, J. Li, H. Wang, X. Huang, B. He, Y. Yao, J. Wang, H. Zhang, H.H. Ngo, W. Guo, A filtration model for prediction of local flux distribution and optimization of submerged hollow fiber membrane module, *AIChE J.* 61 (2015) 4377–4386.

[21] X. Feng, R.Y.-M. Huang, Permeate pressure build-up in shellside-fed hollow fiber pervaporation membranes, *Can. J. Chem. Eng.* 73 (1995) 833–843.

[22] C. Ronco, A. Brendolan, A. Lupi, G. Metry, N.W. Levin, Effects of a reduced inner diameter of hollow fibers in hemodialyzers, *Kidney Int.* 58 (2000) 809–817.

[23] S.-H. Yoon, S. Lee, I.-T. Yeom, Experimental verification of pressure drop models in hollow fiber membrane, *J. Membr. Sci.* 310 (2008) 7–12.

[24] L. Zhuang, H. Guo, P. Wang, G. Dai, Study on the flux distribution in a dead-end outside-in hollow fiber membrane module, *J. Membr. Sci.* 495 (2015) 372–383.

[25] J.M. Thorman, S.-T. Hwang, Compressible flow in permeable capillaries under deformation, *Chem. Eng. Sci.* 33 (1978) 15–20.

[26] J. Gilron, A. Soffer, Knudsen diffusion in microporous carbon membranes with molecular sieving character, *J. Membr. Sci.* 209 (2002) 339–352.

[27] H. Ohashi, H. Ohya, M. Aihara, T. Takeuchi, Y. Negishi, J. Fan, S.I. Semenova, Analysis of a two-stage membrane reactor integrated with porous membrane having Knudsen diffusion characteristics for the thermal decomposition of hydrogen sulfide, *J. Membr. Sci.* 166 (2000) 239–247.

[28] D.M. Ruthven, W.J. DeSisto, S. Higgins, Diffusion in a mesoporous silica membrane: Validity of the Knudsen diffusion model, *Chem. Eng. Sci.* 64 (2009) 3201–3203.

[29] K. Wu, Z. Chen, X. Li, Real gas transport through nanopores of varying cross-section type and shape in shale gas reservoirs, *Chem. Eng. J.* 281 (2015) 813–825.

[30] P.F. Zito, A. Caravella, A. Brunetti, E. Drioli, G. Barbieri, Knudsen and surface diffusion competing for gas permeation inside silicalite membranes, *J. Membr. Sci.* 523 (2017) 456–469.

[31] J. Kuhn, R. Stemmer, F. Kapteijn, S. Kjelstrup, J. Gross, A non-equilibrium thermodynamics approach to model mass and heat transport for water pervaporation through a zeolite membrane, *J. Membr. Sci.* 330 (2009) 388–398.

[32] S. Guo, C. Yu, X. Gu, W. Jin, J. Zhong, C.-L. Chen, Simulation of adsorption, diffusion, and permeability of water and ethanol in NaA zeolite membranes, *J. Membr. Sci.* 376 (2011) 40–49.

[33] T. Carroll, N.A. Booker, Axial features in the fouling of hollow-fibre membranes, *J. Membr. Sci.* 168 (2000) 203–212.